Electronic Research Archive

http://www.aimspress.com/journal/era

ERA, 30(11): 4108–4135.
DOI: 10.3934/era.2022208
Received: 27 June 2022
Revised: 16 August 2022
Accepted: 29 August 2022
Published: 19 September 2022

Research article

Walking dynamics for an ascending stair biped robot with telescopic legs and impulse thrust

Jiarui Chen[1], Aimin Tang[2], Guanfeng Zhou[3], Ling Lin[1] and Guirong Jiang[1,*]

[1] School of Mathematics and Computing Science, Guilin University of Electronic Technology, Guilin 541004, China

[2] Library, Guilin University of Electronic Technology, Guilin 541004, China

[3] School of Electronic Engineering and Automation, Guilin University of Electronic Technology, Guilin 541004, China

* **Correspondence:** Email: grjiang9@163.com; Tel: +8613977387382.

Abstract: In this study, an ascending stair biped robot model with impulse thrust is presented. The biped robot contains a hip joint and two legs with massless telescoping actuator. Impulse thrust is applied at the ankle joint of robot's stance leg to simulate the forward push-off of the ankle during human walking. The nonlinear ascending stair biped model is linearized and a discrete map is obtained. The conditions for the existence and stability of period-1 gait are obtained by means of this discrete map. The expressions of torques to ensure robot walking are derived and Flip bifurcation is investigated. Numerical simulations, such as phase diagram of period-1,2,4 gaits and bifurcation diagram, are given in an example. Theoretical analysis and numerical results obtained in this study provide a theoretical basis for stable walking of ascending stair biped robot with periodic gaits.

Keywords: ascending stair biped robot; impulse thrust; Poincaré map; periodic gait; walking dynamics

1. Introduction

The walking system of biped robot is a complex dynamic system with multi variables and strong coupling, which makes the research of robot in different walking environments challenging. Passive dynamic walking (PDW), which was proposed by McGeer [1], provides new ideas for walking dynamics of biped robot. The passive dynamic walking robot can walk stably on a gentle slope without any input. In recent years, most of the research on walking dynamics concerns robots on downhill or flat road, while only little has addressed robots climbing stairs. The results about robot walking dynamics on downhill or flat road are very rich. For example, bifurcations and the chaotic

behavior of passive dynamic biped robots were discussed in [2], a combination of feedback linearization and finite-time controllers was used to control the walking posture and the stability of the whole behavior was investigated by analysis of a one-dimensional Poincaré map [3]. However, little is known about the walking dynamics of biped robot climbing stairs. This work focuses on biped robot climbing stairs.

Human walking is a complex mechanical motion powered by the activity of numerous muscles. For humanoid robot, it is necessary to consider what kind of drive to compensate energy loss caused by heel strike and make it walk more stably and effectively in different environments [4–6]. Different types of driving forces are added to the ankles of robots to simulate the positive ankle push-off during human walking. For example, Daniel et al. [7] considered a simple model based on spring-mass-running with a compliant ankle joint, Zelik et al. [8] and Chen et al. [9] studied a simple dynamic walking model with feet and series elasticity at the ankle joint. The authors utilized non-instantaneous spring thrust added at the ankle to compensate for collision losses. In recent research, impulsive thrust is considered to provide driving force for robot. This driving force can provide effective power to a compass model on level ground [10, 11]. The results of simple two-dimensional (2-D) models with impulsive thrust show that such thrust (ankle push-off) can minimize energy consumption and is a promising driving method for biped robot [12].

In the past, different kinds of robots, such as wheeled robot [13], tracked robot [14], hexapod robot [15] and so on, have been used to investigate walking dynamics of stair ascending. Bipedal robot, which is closer to human behavior, is considered as an important one investigating walking dynamics of stair ascending. A virtual slope method, which regards the stairs as a virtual slope, was proposed to discuss walking trajectory planning on stairs for biped robots [16]. In 1999, Shih et al. designed a 7-DOF biped robot BR-1 with a simplest bipedal structure, which has two variable-length legs for simulating knee joints of human walking and a translatable balance weight in the body for stair climbing [17]. Its walking stability was insured by large feet and carefully controlling the position of the center of gravity. Figliolini et al. developed a biped robot EP-WAR2 with a suitable binary pneumatic actuation and used external control elements like suction cups to ensure equilibrium of the biped while walking or climbing stairs [18]. For the biped robot with multi joints, the complex structure and multi degrees of freedom make the research of walking dynamics more difficult [19–21]. Moreover, stair ascending, so far, is still studied for biped robot as challengeable topics. The theoretical analysis of dynamic stability during stair ascending has been still scarcely involved.

In the process of climbing stairs, the leg structure of bipedal robot is required to be flexible enough to avoid the scuffing problem between the bottom of the foot and the stairs. Telescopic legs can successfully complete the movement of ascending stairs, for example, Asano discussed a modified mechanism for a parametric excitation using telescopic legs and considered this biped robot to ascent stairs by utilizing the hybrid actuation effect [22]. A unifying framework to study energy-efficient optimal gaits for a bipedal model with telescopic legs and without elastic elements on different support surfaces such as level ground, sloped or staircase is discussed in [23].

There are many research methods and results on the dynamics of robots walking on slope and level ground. For example, stability of periodic gaits, limit cycle, chaos, and bifurcations of robot walking are well investigated [24–27], a method of linearization is used to build Poincaré map for PDW [28,29], linear inverted pendulum model is used to discuss biped robots walking [30]. However, the research on the walking of stair climbing biped robot with telescopic legs and impulse thrust is difficult and very

challenging at present, and most of the research conclusions are numerical results. Non-smooth system exists widely in the real world and has complex dynamic behavior [31]. The model of ascending stair biped robot with telescopic legs and impulse thrust belongs to the category of non-smooth system and needs to be further investigated theoretically. For an ascending stair biped model, the clear dynamic information, such as the transition during different phase of the stair ascending, the dynamic equation during swing phase and so on, is critical to plan the motion of the robot's two legs. Motivated by these facts, walking dynamics of a ascending stair biped robot with telescopic legs and impulse thrust is discussed in this paper. The research focuses on calculation of torque to ensure robot walking and on theoretical analysis of the existence of periodic gaits.

This paper is organized as follows: In Section 2, a model of ascending stair biped robot with telescopic legs and impulse thrust is proposed. Theoretical analysis of complex walking dynamics of the ascending stair biped model is given in Section 3. Simulation results are given in Section 4 and this paper is concluded in Section 5.

2. Model description

The model of ascending stair biped robot, which contains a hip joint and two rigid legs with massless telescoping actuator, is illustrated in Figure 1. The length of supporting leg is L_{st} and the length of non-supporting leg is L_{sw}. For simplicity, we assume that the mass of the biped robot is distributed as three units, namely, ankle joints of two legs (m) and hip joint (m_H), where $m_H \gg m$. The variable-length legs is set to serve as knee joints for ascending stairs. The variables θ and γ represent the angles of the supporting (stance) and non-supporting (swing) leg relative to the ground of vertical, respectively. The length and height of the stair are $2S$ and H , respectively. α is the angle between two legs and is given as $\alpha = \theta - \gamma$.

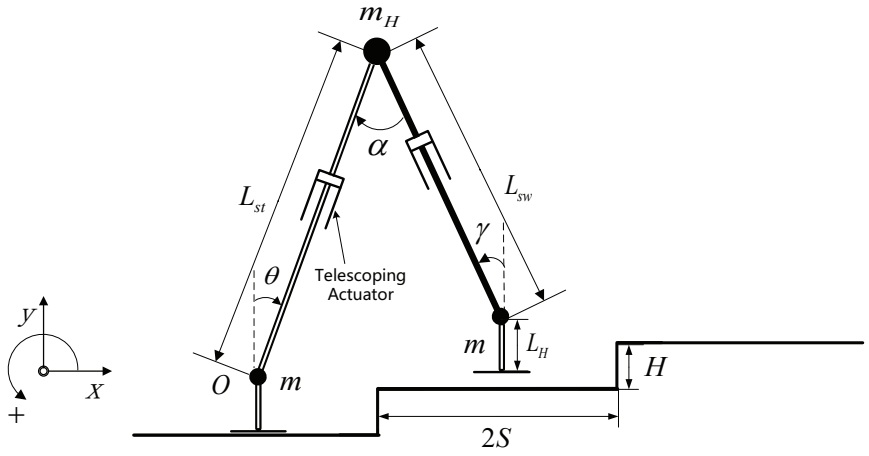

Figure 1. Schematic representation of the model of ascending stair biped robot.

During swing phase, we assume that the frictional coefficient is large enough to prevent sliding between the stance foot and the floor, and the foot of the stance leg is always on the ground. The robot starts from the initial posture with two feet placed in the middle of the stairs and the stride length of the robot is fixed to $2S$. The projection of the hip joint is located at the boundary of the stair. We assume

that the process of collision between the swinging legs and the ground is modeled as the collision of two rigid bodies. After the impact, the stance leg abandons the ground without any interaction with the ground.

The remaining joint below the ankle, which is used to keep balance of the robot during ascending and whose mass is ignored, is called the heel of the ascending stair biped. The mass of telescoping actuator is merged into that of ankle joint. The actuator can make the leg stretch to a specific length in a short time, while not generating additional impulse force to make the leg bounce from the ground.

2.1. Four-phase gait

As shown in Figure 2, the four phases separate one step into two continuous phases and two instantaneous process, namely, the swing phase before stretching of the stance leg (I and II), the instantaneous stretching phase of the stance leg (II and III), the swing phase after stretching of the stance leg (III and IV), the impact conditions (IV).

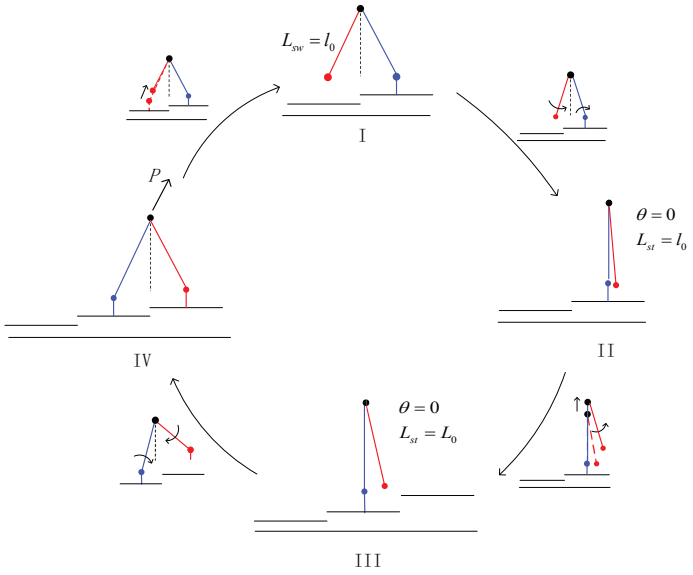

Figure 2. The walking process of one step of ascending stair biped robot. The stance leg is represented in blue and the swing leg is represented in red. The black arrow on the swing leg indicates the swing direction of the leg.

Let $q = \begin{bmatrix} \theta & \gamma \end{bmatrix}$ be the vector of generalized coordinates of the ascending stair biped model. The two continuous phases of bipedal robot walking model can be represented by the following nonlinear differential equations according to the Lagrangian dynamics.

$$F_i = \frac{d}{dt}\frac{\partial L}{\partial \dot{q}_i} - \frac{\partial L}{\partial q_i}, \tag{1}$$

where $L(q, \dot{q}) = K(q, \dot{q}) - V(q)$ is the Lagrange equation defined by the kinetic energy (K) and potential energy (V) in the system. F_i is the generalized force applied to the mass points.

At the instantaneous stretching phase of the stance leg and the impact instant with the stair, the state variable of the system undergo two transient variations according to the law of conservation of angular momentum.

The first phase(I–II). The bipedal robot starts climbing with the initial state, namely, $\theta = \theta_0$, $\gamma = \gamma_0$ and $L_{st} = L_{sw} = l_0$. The behavior of this phase is similar to that of swing phase of a simple two link biped. This phase lasts until $\theta = 0$ (the stance leg perpendicular to the stair). It follows from (1) that

$$M_1(q)\ddot{q} + C_1(q,\dot{q})\dot{q} + G_1(q) = B_1 u, \tag{2}$$

where M_1 is the inertia matrix, C_1 includes Coriolis and centrifugal terms, G_1 includes gravity forces, B_1 is the input matrix, u is the torque vector. They are given as follows.

$$M_1(q) = \begin{bmatrix} (1+\rho){l_0}^2 & -\rho {l_0}^2 \cos(\theta-\gamma) \\ -{l_0}^2\cos(\theta-\gamma) & {l_0}^2 \end{bmatrix},$$

$$C_1(q,\dot{q}) = \begin{bmatrix} 0 & -\rho {l_0}^2 \sin(\theta-\gamma)\dot{\gamma} \\ {l_0}^2\sin(\theta-\gamma)\dot{\theta} & 0 \end{bmatrix},$$

$$G_1(q) = \begin{bmatrix} -g(1+\rho)l_0\sin\theta \\ g l_0 \sin\gamma \end{bmatrix}, \quad B_1 = \frac{1}{m_H}\begin{bmatrix} 0 & -1 \\ \frac{1}{\rho} & \frac{1}{\rho} \end{bmatrix}, \quad u = \begin{bmatrix} u_1 & u_2 \end{bmatrix}^T,$$

where $\rho = \frac{m}{m_H}$, the torques u_1 and u_2 are applied to the hip joint and the ankle joints of stance during this phase, respectively.

The second phase (II and III). The instantaneous phase occurs when the stance leg perpendicular to the stair, which is defined by the following set.

$$\overline{HS_1} = \left\{ q \in \mathbb{R}^2 : \theta = 0 \right\}. \tag{3}$$

There is no change in the angular momentum just before and after the stretching phase and the length of the stance leg is varied from l_0 to L_0, where L_0 is the maximum leg length. The transition rules at the moment are given as follows.

$$q^+ = q^-, \quad \dot{q}^+ = Se(q^-)\dot{q}^-, \tag{4}$$

where the subscripts and represent just after and just before this instantaneous phase, respectively. $Se(q) = (Q_1^+(\alpha))^{-1}Q_1^-(\alpha)$ with $\alpha = \theta^- - \gamma^- = \theta^+ - \gamma^+$,

$$Q_1^- = \begin{bmatrix} (1+\rho){l_0}^2 - \rho {l_0}^2\cos(\alpha) & \rho {l_0}^2(1-\cos(\alpha)) \\ -{l_0}^2\cos(\alpha) & {l_0}^2 \end{bmatrix},$$

and

$$Q_1^+ = \begin{bmatrix} (1+\rho)L_0^2 - \rho l_0 L_0\cos(\alpha) & \rho {l_0}^2(1-\cos(\alpha)) \\ -l_0 L_0\cos(\alpha) & {l_0}^2 \end{bmatrix}.$$

The third phase (III and IV). The stance leg continues swinging around the ankle joint until the swing leg and the stair are about to collide. Unlike first phase, the two legs are not equal in length in this phase. The dynamics of this phase can be expressed as follows.

$$M_2(q)\ddot{q} + C_2(q,\dot{q})\dot{q} + G_2(q) = B_2 u, \tag{5}$$

where

$$M_2(q) = \begin{bmatrix} L_0^2 + \rho {l_0}^2 & -\rho l_0 L_0\cos(\theta-\gamma) \\ -l_0 L_0\cos(\theta-\gamma) & {l_0}^2 \end{bmatrix}, \quad u = \begin{bmatrix} u_3 & u_4 \end{bmatrix}^T,$$

$$C_2(q,\dot{q}) = \begin{bmatrix} 0 & -\rho l_0 L_0 \sin(\theta-\gamma)\dot{\gamma} \\ l_0 L_0 \sin(\theta-\gamma)\dot{\theta} & 0 \end{bmatrix},$$

$$G_2(q) = \begin{bmatrix} -g(1+\rho)L_0 \sin\theta \\ g l_0 \sin\gamma \end{bmatrix}, \quad B_2 = \frac{1}{m_H}\begin{bmatrix} 0 & 1 \\ -\frac{1}{\rho} & -\frac{1}{\rho} \end{bmatrix}.$$

The forth phase (IV). In this instantaneous process, in order to let the biped robot have enough energy during the next period gait, we apply impulse force p on the the stance leg, which follows the direction of this leg. Moreover, for avoiding the scuffing problem, the length of the new swing leg is shortened to l_0 at the moment of role switch between the two legs, as well as its heel is retracted. The impact phase occurs for the three following mathematical conditions are satisfied.

$$\overline{HS_2} = \begin{cases} \Upsilon_1(q) = L_0\cos\theta - l_0\cos\gamma = H, \\ \Upsilon_2(q,\dot{q}) = l_0\dot{\gamma}\sin\gamma - L_0\dot{\theta}\sin\theta < 0, \\ \Upsilon_3(q) = l_0\sin\gamma - L_0\sin\theta = 2S, \end{cases} \tag{6}$$

where $\Upsilon_2(q,\dot{q}) = \frac{d\Upsilon_1(q)}{dt} = \frac{\partial\Upsilon_1(q)}{\partial q}\dot{q}$. Condition (6) ensures that the swing leg reaches the stair, is moving downward, and is in front of the stance leg and the mass points of two legs are $2S$ apart.

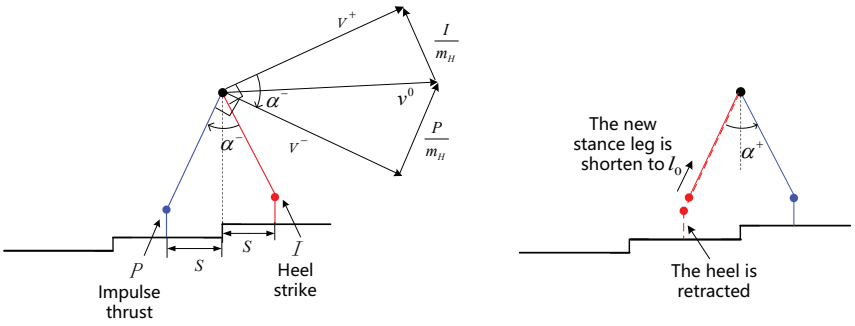

(a) (b)

Figure 3. Instantaneous collision switching model for bipedal robots, (a) the moment of just before role switch between two legs, (b) the moment of just after role switch between the two legs. The length of the new swing leg is shortened to l_0 and its heel is retracted.

In this impact phase, impulse thrust p along the direction of the stance leg is used to provide the power. Instantaneous collision switching model for bipedal robots with impulse thrust is shown in Figure 3. One can calculate that

$$L_0 = \sqrt{\left(\sqrt{l_0^2 - S^2} + H\right)^2 + S^2}, \tag{7}$$

$$\theta^- = \gamma^+ = -\arcsin\frac{S}{L_0}, \gamma^- = \theta^+ = \arcsin\frac{S}{l_0}.$$

It follows from $v^+ = l_0\dot{\theta}^+, v^- = L_0\dot{\theta}^-$ that

$$\dot{\theta}^+ = \frac{L_0}{l_0}\dot{\theta}^-\cos(\theta^- - \gamma^-) + \frac{p}{m_H l_0}\sin(\theta^- - \gamma^-).$$

According to the momentum theorem, the following algebraic expression is obtained.

$$\dot{\gamma}^+ = (1 - \frac{L_0}{l_0} + \frac{l_0}{L_0})\dot{\theta}^+\cos(\theta^+ - \gamma^+).$$

The transition of the impact phase can be expressed as follows.

$$\begin{bmatrix} \theta \\ \gamma \\ \dot{\theta} \\ \dot{\gamma} \end{bmatrix}^{+} = \begin{bmatrix} 0 & 1 & 0 & 0 \\ 1 & 0 & 0 & 0 \\ 0 & 0 & s_{33} & 0 \\ 0 & 0 & s_{43} & 0 \end{bmatrix} \begin{bmatrix} \theta \\ \gamma \\ \dot{\theta} \\ \dot{\gamma} \end{bmatrix}^{-} + \begin{bmatrix} 0 \\ 0 \\ w_3 \\ w_4 \end{bmatrix} p, \tag{8}$$

where $s_{33} = \frac{L_0}{l_0}\cos(\alpha^-)$, $s_{43} = (1 - \frac{L_0}{l_0} + \frac{l_0}{L_0})\cos(\alpha^+)s_{33}$, $w_3 = \frac{1}{m_H l_0}\sin(\alpha^-)$, and $w_4 = \frac{(1-\frac{L_0}{l_0}+\frac{l_0}{L_0})}{m_H l_0}\sin(\alpha^-)\cos(\alpha^+)$.

2.2. Impulsive hybrid nonlinear dynamics

Equations (2), (4), (5) and (8) and conditions (3) and (6) represent different parts of the walking dynamics of ascending stair biped model in one step. Thus the complete walking dynamics of the ascending stair biped model can be represented as an impulsive hybrid system consisting of multiple continuous nonlinear differential equations and multiple discrete algebraic mappings.

Let $X = (q\ \dot{q})^T = (\theta\ \gamma\ \dot{\theta}\ \dot{\gamma})^T = (x_1\ x_2\ x_3\ x_4)^T$ be the state vector. In view of (2)–(8), the impulsive hybrid system is described as follows.

$$\begin{cases} \dot{X} = f_1(X), & X \in \Omega_1, \\ X^+ = \Delta_1(X^-), & X^- \in HS_1, \\ \dot{X} = f_2(X), & X \in \Omega_2, \\ X^+ = \Delta_2(X^-) + g(X^-)p, & X^- \in HS_2, \end{cases} . \tag{9}$$

where

$$f_i(X) = \begin{bmatrix} \dot{q} \\ -M_i(q)^{-1}\left(C_i(q,\dot{q}) + G_i(q) - B_i u\right) \end{bmatrix}, \quad i = 1, 2,$$

$$\Delta_1(X) = \begin{bmatrix} I_{2\times 2} & O_{2\times 2} \\ O_{2\times 2} & Se(X) \end{bmatrix} X, \quad \Delta_2(X) = \begin{bmatrix} 0 & 1 & 0 & 0 \\ 1 & 0 & 0 & 0 \\ 0 & 0 & s_{33} & 0 \\ 0 & 0 & s_{43} & 0 \end{bmatrix} X, \quad g = \begin{bmatrix} 0 \\ 0 \\ w_3 \\ w_4 \end{bmatrix},$$

$$\begin{aligned} HS_1 &= \left\{X \in \mathbb{R}^4 | \mathrm{G}(X) = x_1 = 0\right\}, \\ HS_2 &= \{X \in \mathbb{R}^4 |\ \Upsilon_1(X) = h, \quad \Upsilon_2(X) < 0, \quad \Upsilon_3(X) = 2S\ \}. \end{aligned} \tag{10}$$

Ω_1 and Ω_2 denote the state space of the swing phase before and after stretching of the stance leg, respectively.

3. Dynamical analysis

3.1. Poincaré map

Choose the following hyperplane as the Poincaré section.

$$\Sigma = \left\{X \in \mathbb{R}^4 | x_1 = \arcsin\tfrac{S}{l_0},\ x_2 = -\arcsin\tfrac{S}{L_0}\right\}. \tag{11}$$

Let $X_k = \left(\arcsin\frac{S}{l_0},\ -\arcsin\frac{S}{L_0},\ x_{3k},\ x_{4k}\right)^T$ be the initial point of $X(t)$, where $X_k = X(0) \in \Sigma$.

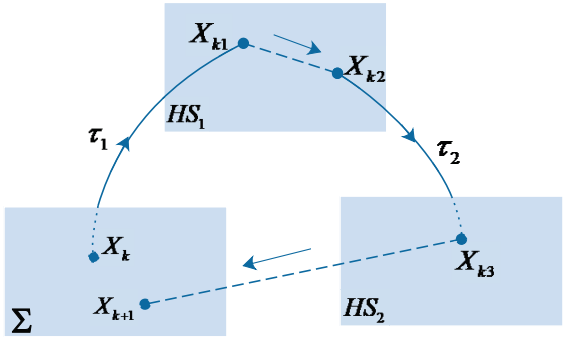

Figure 4. The trajectory $X(t)$ of system (9) starting from the initial point X_k and returning to Poincaré section Σ.

As shown in Figure 4, the trajectory $X(t)$ starting from X_k reaches the point $X_{k1} = (0,\ x_{2k1},\ x_{3k1},\ x_{4k1})^T = X(\tau_1)$ at $t = \tau_1$, and jumps to $X_{k2} = (0,\ x_{2k2},\ x_{3k2},\ x_{4k2})^T = X(\tau_1^+)$ in the plane HS_1, where $X_{k2} = \Delta_1(X_{k1})$.

The trajectory $X(t)$ reaches the point $X_{k3} = \left(-\arcsin\frac{S}{L_0},\ \arcsin\frac{S}{l_0},\ x_{3k3},\ x_{4k3}\right)^T$ in the plane HS_2 at $t = \tau_1 + \tau_2$ under the action of torques, where $X_{k3} = X(\tau_1 + \tau_2)$. Then it jumps to $X_{k+1} = \left(\arcsin\frac{S}{l_0},\ -\arcsin\frac{S}{L_0},\ x_{3(k+1)},\ x_{4(k+1)}\right)^T$ in Poincaré section Σ due to the effect of impulse thrust p and role exchange of two legs.

Hence we obtain the following Poincaré map.

$$X_{k+1} = F(X_k). \tag{12}$$

However, due to the fact that the impulsive hybrid nonlinear dynamics of the system (9) includes two nonlinear differential equations, it is difficult to obtain explicit expression of τ_1, τ_2, and solutions to (9) , especially to ensure the trajectory $X(t)$ intersects the plane HS_2 at $t = \tau_1 + \tau_2$, namely, the two conditions $x_1(\tau_1 + \tau_2) = -\arcsin\frac{S}{L_0}$ and $x_2(\tau_1 + \tau_2) = \arcsin\frac{S}{L_0}$ hold at the same time. Hence, the Poincaré map (12) can be used for numerically simulation of the complex dynamic behavior of system (9), but not for theoretical analysis of walking dynamics. In order to solve the above problems, we linearize system (9), obtain an explicit map, and discuss the walking dynamics of ascending stair biped robot.

3.2. Linearized system

For simplicity, we denote basic unit ι by $\iota \triangleq \sqrt{\frac{l_0}{g}}$. By dimensionless and linearizing the Eqs (2) and (5) around the equilibrium point $q = \dot{q} = O_{2\times 2}$, we have

$$\begin{cases} \ddot{\theta} - \theta = -u_2^* \\ \ddot{\gamma} - (\theta - \gamma) = \frac{u_1^* + u_2^*}{\rho} - u_2^* \end{cases},$$

$$\begin{cases} \ddot{\theta} - \frac{g}{L_0}\theta = u_4^* \\ \ddot{\gamma} - (\theta - \gamma) = \frac{-u_3^* - \frac{1}{d_1^2}u_4^*}{\rho} + \frac{L_0}{g}u_4^* \end{cases}.$$

where $u_i^* = \frac{u_i}{l_0^2 m_H}(i = 1, 2, 3)$, $u_4^* = \frac{u_4}{L_0^2 m_H}$, $d_1 = \frac{l_0}{L_0}$.

Hence system (9) can be rewritten as

$$\begin{cases} \dot{X} = \left(x_3(t), x_4(t), x_1(t) - u_2^*, x_1(t) - x_2(t) + \frac{u_1^* + u_2^*}{\rho} - u_2^*\right)^T, & X \in \Omega_1, \\ X^+ = \tilde{\Delta}_1(X^-), & X^- \in HS_1, \\ \dot{X} = \left(x_3(t), x_4(t), \frac{g}{L_0}x_1(t) + u_4^*, x_1(t) - x_2(t) + \frac{-u_3^* - \frac{1}{d_1^2}u_4^*}{\rho} + \frac{L_0}{g}u_4^*\right)^T, & X \in \Omega_2, \\ X^+ = \Delta_2(X^-) + g(X^-)p, & X^- \in HS_2, \end{cases} \tag{13}$$

where $\tilde{\Delta}_1(x) = \begin{bmatrix} I_{2\times 2} & O_{2\times 2} \\ O_{2\times 2} & \tilde{S}e(x) \end{bmatrix} x$, $\tilde{S}e = \begin{bmatrix} L_0^2 & 0 \\ -l_0 L_0 \cos(\alpha) & l_0^2 \end{bmatrix}^{-1} \begin{bmatrix} l_0^2 & 0 \\ -l_0^2 \cos(\alpha) & l_0^2 \end{bmatrix}$, and the input torques $u_2^* = e_2$, and $u_4^* = e_4$ are constant.

3.3. Realization of climbing stairs

Now set the initial point as $A_k^+ = (\theta_0,\ \gamma_0,\ x_{3k0},\ x_{4k0})^T$, where $x_{4k0} = \cos\alpha_0(1 - \frac{1}{d_1} + d_1)x_{3k0}$, $\alpha_0 = \theta_0 - \gamma_0$, x_{3k0} represents the initial angular velocity of the kth step of the robot's stance leg. As shown in Figure 5, the trajectory of system (13) starting from A_k^+ reaches the point $B_k^-(0,\ x_2(\tau_1),\ x_3(\tau_1),\ x_4(\tau_1))^T$ in HS_1 at $t = \tau_1$, and jumps to B_k^+ via the algebraic equation in (13), where

$$B_k^+ = (0,\ x_2(\tau_1),\ d_1^2 x_3(\tau_1),\ \cos\alpha_1(d_1 - 1)x_3(\tau_1) + x_4(\tau_1))^T,$$

and $\alpha_1 = x_1(\tau_1) - x_2(\tau_1) = -x_2(\tau_1)$.

For $t \in [0, \tau_1]$, the solution of (13) is

$$\begin{cases} x_1(t) = \frac{\theta_0 - e_2 + x_{3k0}}{2}e^t + \frac{\theta_0 - e_2 - x_{3k0}}{2}e^{-t} + e_2, \\ x_2(t) = \left(\gamma_0 - \frac{u_1^* + e_2}{\rho} - \frac{\theta_0 - e_2}{2}\right)\cos t + \left((1 - \frac{1}{d_1} + d_1)\cos\alpha_0 - \frac{1}{2}\right)x_{3k0}\sin t \\ \quad + \frac{\theta_0 - e_2 + x_{3k0}}{4}e^t + \frac{\theta_0 - e_2 - x_{3k0}}{4}e^{-t} + \frac{u_1^* + e_2}{\rho}, \\ x_3(t) = \frac{\theta_0 - e_2 + x_{3k0}}{2}e^t - \frac{\theta_0 - e_2 - x_{3k0}}{2}e^{-t}, \\ x_4(t) = -\left(\gamma_0 - \frac{u_1^* + e_2}{\rho} - \frac{\theta_0 - e_2}{2}\right)\sin t + \left((1 - \frac{1}{d_1} + d_1)\cos\alpha_0 - \frac{1}{2}\right)x_{3k0}\cos t \\ \quad + \frac{\theta_0 - e_2 + x_{3k0}}{4}e^t - \frac{\theta_0 - e_2 - x_{3k0}}{4}e^{-t}. \end{cases} \tag{14}$$

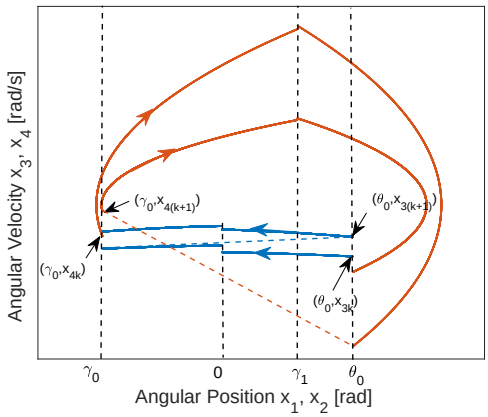

Figure 5. The solution of system (13) from the initial point $A_k = (\theta_0,\ \gamma_0,\ x_{3k0},\ x_{4k0})^T$ in $x_1\,(x_3) - x_2\,(x_4)$ space.

It follows from $\mathrm{T}(x(\tau_1)) = x_1(\tau_1) = 0$ that

$$\tau_1 = \ln \frac{-e_2 - \sqrt{x_{3k0}^2 - \theta_0^2 + 2\theta_0 e_2}}{\theta_0 - e_2 + x_{3k0}}. \tag{15}$$

For convenient calculation and analysis, assume $x_2(\tau_1) = \gamma_1$ is constant under the action of unknown torque u_1^* and definite torque $u_2^* = e_2$. So we obtain

$$\begin{aligned} u_1^* = \Big[\gamma_1 - \Big(\gamma_0 - \tfrac{e_2}{\rho} - \tfrac{\theta_0 - e_2}{2}\Big)\cos\tau_1 \\ - \cos\alpha_0 \Big((1 - \tfrac{1}{d_1} + d_1) - \tfrac{1}{2}\Big) x_{3k0} \sin\tau_1 + \tfrac{\rho-2}{2\rho} e_2\Big] \tfrac{\rho}{1-\cos\tau_1}. \end{aligned} \tag{16}$$

Suppose that the trajectory reaches the point $A_{k+1}^- = (\gamma_0,\ \theta_0,\ x_3(\tau_1 + \tau_2),\ x_4(\tau_1 + \tau_2))$ in the plane HS_2 at $t = \tau_1 + \tau_2$, and jumps to A_{k+1}^+. Similarly, for $t \in (\tau_1, \tau_1 + \tau_2]$, the solution of (13) is

$$\begin{cases} x_1(t) = C_5 e^{\sqrt{\frac{g}{L_0}}(t-\tau_1)} + C_6 e^{-\sqrt{\frac{g}{L_0}}(t-\tau_1)} - \frac{L_0}{g} e_4, \\ x_2(t) = C_7 \cos(t-\tau_1) + C_8 \sin(t-\tau_1) - \dfrac{1}{d_1^2 \rho} e_4 - \dfrac{1}{\rho} u_3^* \\ \qquad\qquad + \frac{L_0}{L_0+g}(C_5 e^{\sqrt{\frac{g}{L_0}}(t-\tau_1)} + C_6 e^{-\sqrt{\frac{g}{L_0}}(t-\tau_1)}), \\ x_3(t) = \sqrt{\frac{g}{L_0}} C_5 e^{\sqrt{\frac{g}{L_0}}(t-\tau_1)} - \sqrt{\frac{g}{L_0}} C_6 e^{-\sqrt{\frac{g}{L_0}}(t-\tau_1)}, \\ x_4(t) = -C_7 \sin(t-\tau_1) + C_8 \cos(t-\tau_1) \\ \qquad\qquad + \frac{L_0}{L_0+g}\sqrt{\frac{g}{L_0}}(C_5 e^{\sqrt{\frac{g}{L_0}}(t-\tau_1)} - C_6 e^{-\sqrt{\frac{g}{L_0}}(t-\tau_1)}), \end{cases} \tag{17}$$

where

$$C_5 = \frac{L_0}{2g} e_4 - Z_1,\ C_6 = \frac{L_0}{2g} e_4 + Z_1,$$

$$C_7 = Z_2 \cos\tau_1 + Z_3 \sin\tau_1 + Z_5,\ C_8 = -Z_2 \sin\tau_1 + Z_3 \cos\tau_1 + Z_6,$$

$$Z_1 = \frac{d_1^2}{2}\sqrt{\frac{L_0}{g}}\sqrt{x_{3k0}^2 - \theta_0^2 + 2\theta_0 e_2},\ Z_2 = \gamma_0 - \frac{u_1^* + e_2}{\rho} - \frac{\theta_0 - e_2}{2},$$

$$Z_3 = \cos\alpha_0\left((1-\frac{1}{d_1}+d_1)-\frac{1}{2}\right)x_{3k0},\ Z_5 = -\frac{e_2}{2}+\frac{u_1^*+e_2}{\rho}+Z_4e_4+\frac{1}{\rho}u_3^*,$$

$$Z_4 = -\frac{L_0^2}{g\,(L_0+g)}+\frac{1}{d_1^2\rho},\ Z_6 = \left(\frac{l_0^2}{(L_0+g)L_0}-(d_1-1)\cos\alpha_1-\frac{1}{2}\right)\sqrt{x_{3k0}^2-\theta_0^2+2\theta_0e_2},$$

$$Z_7 = \frac{L_0}{L_0+g}(\frac{L_0}{2g}e_4-Z_1),\ Z_8 = \frac{L_0}{L_0+g}(\frac{L_0}{2g}e_4+Z_1).$$

It follows from $A_{k+1}^- = (\gamma_0,\ \theta_0,\ x_3(\tau_1+\tau_2),\ x_4(\tau_1+\tau_2))^T \in HS_2$ that $x_1(\tau_1+\tau_2) = \gamma_0$ and $x_2(\tau_1+\tau_2) = \theta_0$. Hence

$$\tau_2 = \sqrt{\frac{L_0}{g}}\ln\frac{\gamma_0+\frac{L_0}{g}e_4-\sqrt{4Z_1^2+\gamma_0^2+2\gamma_0\frac{L_0}{g}e_4}}{\frac{L_0}{g}e_4-2Z_1}, \tag{18}$$

$$\begin{aligned} u_3^* = \Big[&\theta_0-\tfrac{L_0}{L_0+g}\gamma_0+Z_4e_4-(-Z_2\sin\tau_1+Z_3\cos\tau_1+Z_6)\sin\tau_2\\ &-(Z_2\cos\tau_1+Z_3\sin\tau_1-\tfrac{e_2}{2}+\tfrac{u_1^*+e_2}{\rho}+Z_4e_4)\cos\tau_2\Big]\tfrac{\rho}{\cos\tau_2-1}\end{aligned}. \tag{19}$$

Set the values of the torques u_1^* and u_3^* according to conditions (16) and (19). It follows that $x_1(\tau_1+\tau_2) = \gamma_0$ and $x_2(\tau_1+\tau_2) = \theta_0$ hold at the same time, which enables two legs to exchange smoothly and ensures the realization of climbing stairs. The following result is obtained.

Proposition 1. *Given the values of torque u_2^* and u_4^* in system (13) and set the initial point as $A_k^+ = (\theta_0,\ \gamma_0,\ x_{3k0},\ x_{4k0})^T$, where $x_{4k0} = \cos\alpha_0(1-\frac{1}{d_1}+d_1)x_{3k0}$. To ensure the realization of climbing stairs, the torque u_1^* and u_3^* are determined by (16) and (19), respectively. The time of each step is $\tau_1+\tau_2$, where τ_1 and τ_2 are shown in (15) and (18), respectively.*

3.4. Existence of periodic gaits

In the above subsection, $A_{k+1}^- = (\gamma_0,\ \theta_0,\ x_3(\tau_1+\tau_2),\ x_4(\tau_1+\tau_2))^T$ in the plane HS_2. It follows from A_{k+1}^- and $X^+ = \Delta_2(X^-)+g(X^-)p$ $(X^- \in HS_2)$ that

$$\begin{aligned} A_{k+1}^+ = \Big(&\theta_0,\ \gamma_0,\ \tfrac{\cos(-\alpha_0)}{d_1}x_3(\tau_1+\tau_2)+\tfrac{p}{m_Hl_0}\sin(-\alpha_0),\\ &\cos\alpha_0(1-\tfrac{1}{d_1}+d_1)[\tfrac{1}{d_1}\cos(-\alpha_0)x_3(\tau_1+\tau_2)+\tfrac{p}{m_Hl_0}\sin(-\alpha_0)]\Big)^T,\end{aligned}$$

where $x_3(\tau_1+\tau_2) = -\sqrt{\frac{4g}{L_0}Z_1^2+\frac{g}{L_0}\gamma_0^2+2\gamma_0e_4}$.

The previous literature considered the constant impulse thrust [10, 11], but the change of velocity should be considered in the implementation of impulse thrust. Since the impulse thrust is constrained by control amplitude [32], we consider the following impulse thrust with velocity dependent and amplitude constraint.

$$p = b\,|\sin x_{3k0}| + c, \tag{20}$$

where $b \in \mathbb{R}$, $c \in \mathbb{R}$, and $|p| \le |b|+|c|$.

Together with the points A_k^+ and A_{k+1}^+, we obtain the following result.

$$\begin{cases} x_{3(k+1)0} = \frac{b|\sin x_{3k0}|+c}{m_Hl_0}\sin(-\alpha_0)-\frac{\cos(-\alpha_0)}{d_1}\sqrt{\frac{4g}{L_0}Z_1^2+\frac{g}{L_0}\gamma_0^2+2\gamma_0e_4},\\ x_{4(k+1)0} = \cos\alpha_0(1-\frac{1}{d_1}+d_1)x_{3(k+1)0},\end{cases}$$

where $Z_1 = \frac{d_1^2}{2}\sqrt{\frac{L_0}{g}}\sqrt{x_{3k0}^2 - \theta_0^2 + 2\theta_0 e_2}$.

Now consider the following map.

$$x_{3(k+1)0} = \frac{b\,|\sin x_{3k0}| + c}{m_H l_0}\sin(-\alpha_0) - \frac{\cos(-\alpha_0)}{d_1}\sqrt{\frac{4g}{L_0}Z_1^2 + \frac{g}{L_0}\gamma_0^2 + 2\gamma_0 e_4}, \tag{21}$$

Let the fixed point of map (21) is x_{3d}, then

$$x_{3d} = \frac{b\,|\sin x_{3d}| + c}{m_H l_0}\sin(-\alpha_0) - \frac{\cos(-\alpha_0)}{d_1}\sqrt{\frac{4g}{L_0}Z_1^2 + \frac{g}{L_0}\gamma_0^2 + 2\gamma_0 e_4},$$

where $Z_1 = \frac{d_1^2}{2}\sqrt{\frac{L_0}{g}}\sqrt{x_{3d}^2 - \theta_0^2 + 2\theta_0 e_2}$.

One fixed point s_d of map (21) corresponds to one periodic gait of (13), which starts from the point $A_k^+ = (\theta_0,\ \gamma_0,\ x_{3d},\ x_{4d})^T$ and returns to the point A_k^+ after time $\tau_{1d} + \tau_{2d}$ under the action of torques u_{1d}^* and u_{3d}^*, where $x_{4d} = \cos\alpha_0(1 - \frac{1}{d_1} + d_1)x_{3d}$,

$$\tau_{1d} = \ln\frac{-e_2 - \sqrt{x_{3d}^2 - \theta_0^2 + 2\theta_0 e_2}}{\theta_0 - e_2 + x_{3d}},$$

$$\tau_{2d} = \sqrt{\frac{L_0}{g}}\ln\frac{\gamma_0 + \frac{L_0}{g}e_4 - \sqrt{4Z_1^2 + \gamma_0^2 + 2\gamma_0\frac{L_0}{g}e_4}}{\frac{L_0}{g}e_4 - 2Z_1},$$

$$\begin{aligned}
u_{1d}^* = &\Big[\gamma_1 - \Big(\gamma_0 - \tfrac{e_2}{\rho} - \tfrac{\theta_0 - e_2}{2}\Big)\cos\tau_{1d} \\
&- \cos\alpha_0\Big((1 - \tfrac{1}{d_1} + d_1) - \tfrac{1}{2}\Big)x_{3d}\sin\tau_{1d} + \tfrac{\rho-2}{2\rho}e_2\Big]\tfrac{\rho}{1-\cos\tau_{1d}}, \\
u_{3d}^* = &\Big[\theta_0 - \tfrac{L_0}{L_0+g}\gamma_0 + Z_4 e_4 - (-Z_2\sin\tau_{1d} + Z_3\cos\tau_{1d} + Z_6)\sin\tau_{2d} \\
&-(Z_2\cos\tau_{1d} + Z_3\sin\tau_{1d} - \tfrac{e_2}{2} + \tfrac{u_{1d}^* + e_2}{\rho} + Z_4 e_4)\cos\tau_{2d}\Big]\tfrac{\rho}{cos\tau_{2d}-1}.
\end{aligned}$$

In particular, set $e_2 = \frac{\theta_0}{2}$, $e_4 = -\frac{\gamma_0}{2d_2^2}$ $(\gamma_0 < 0)$ in (13), where $d_2 = \sqrt{\frac{L_0}{g}}$. It follows from map (21) that

$$x_{3(k+1)0} = -\cos(-\alpha_0)d_1\,|x_{3k0}| + \frac{b\,|\sin x_{3k0}| + c}{m_H l_0}\sin(-\alpha_0) = h(x_{3k0}). \tag{22}$$

Note that $x_{3d} < 0$ and $\alpha_0 \in \left(0,\ \frac{\pi}{2}\right)$, the fixed point of map (22) is the solution of equation

$$x_{3d} = d_1\cos\alpha_0\ x_{3d} - \tfrac{b|\sin x_{3d}| + c}{m_H l_0}\sin\alpha_0. \tag{23}$$

Now construct a function $\sigma_1(y)$ as follows.

$$\sigma_1(y) = (1 - d_1\cos\alpha_0)\,y + \tfrac{b|\sin y| + c}{m_H l_0}\sin\alpha_0, \tag{24}$$

where $c \in (0,\ +\infty)$.

For $y = 0$,

$$\sigma_1(0) = \tfrac{c}{m_H l_0}\sin\alpha_0 > 0. \tag{25}$$

For $y = -\frac{\pi}{2}$,

$$\sigma_1(-\tfrac{\pi}{2}) = -\tfrac{\pi}{2}(1 - d_1\cos\alpha_0) + \tfrac{b+c}{m_H l_0}\sin\alpha_0 < 0, \tag{26}$$

under condition

$$b < -c + \frac{\pi m_H l_0}{2\sin\alpha_0}(1 - d_1\cos\alpha_0) := b_1. \tag{27}$$

The function $\sigma_1(y)$ is continuous for $y \in \left[-\frac{\pi}{2}, 0\right]$. It follows from

$$b < \frac{m_H l_0}{\sin\alpha_0}(1 - d_1\cos\alpha_0) := b_2, \tag{28}$$

that

$$\sigma_1{}'(y) = (1 - d_1\cos\alpha_0) - \frac{b\cos y}{m_H l_0}\sin\alpha_0 > 0.$$

So $\sigma_1(y)$ is a monotonically increasing function and there is only one root of equation $\sigma_1(y) = 0$ for $b < \min\{b_1,\ b_2\}$. There is an unique fixed point in map (22) and hence there is an unique periodic gait in system (13) for $e_2 = \frac{\theta_0}{2}$, $e_4 = -\frac{\gamma_0}{2d_2^2}$ ($\gamma_0 < 0$), and $b < \min\{b_1,\ b_2\}$. Thus we obtain the following result.

Proposition 2. *Set $e_2 = \frac{\theta_0}{2}$, $e_4 = -\frac{\gamma_0}{2d_2^2}$ in system (13). There is an unique periodic gait for $b < \min\{b_1,\ b_2\}$, where b_1 and b_2 are shown in (27) and (28), respectively.*

Now expand the range of parameter e_4 and discuss existence of periodic solution of system (13). Set $e_2 = \frac{\theta_0}{2}$, $e_4 \in \left(\frac{\gamma_0}{2d_2^2},\ 0\right)$. The fixed point of map (21) is the solution of the following equation.

$$x_{3d} = -\frac{\cos\alpha_0}{d_1}\sqrt{{d_1}^4 x_{3d}^2 + 2\gamma_0 e_4 + \frac{\gamma_0^2}{d_2^2}} - \frac{b|\sin x_{3d}| + c}{m_H l_0}\sin\alpha_0. \tag{29}$$

Construct function $\sigma_2(y)$ as follows.

$$\sigma_2(y) = y + \frac{\cos\alpha_0}{d_1}\sqrt{{d_1}^4 y^2 + 2e_4\gamma_0 + \frac{\gamma_0^2}{d_2^2}} + \frac{b|\sin y| + c}{m_H l_0}\sin\alpha_0, \tag{30}$$

where $c \in \left(0,\ -\left[-\frac{\pi}{2} + \frac{\cos\alpha_0}{d_1}\sqrt{\frac{\pi^2 {d_1}^4}{4} + \frac{2\gamma_0^2}{d_2^2}}\right]\frac{m_H l_0}{\sin\alpha_0}\right)$ and $\alpha_0 \in \left(0,\ \frac{\pi}{2}\right)$.

It follows from $e_4 \in \left(\frac{\gamma_0}{2d_2^2}, 0\right)$ that

$$\frac{2\gamma_0^2}{d_2^2} > 2\gamma_0 e_4 + \frac{\gamma_0^2}{d_2^2} > \frac{\gamma_0^2}{d_2^2} > 0, \tag{31}$$

and

$$\begin{aligned}
\sigma_2(y) &= y + \frac{\cos\alpha_0}{d_1}\sqrt{{d_1}^4 y^2 + 2e_4\gamma_0 + \frac{\gamma_0^2}{d_2^2}} + \frac{b|\sin y| + c}{m_H l_0}\sin\alpha_0 \\
&> y + \frac{\cos\alpha_0}{d_1}\sqrt{{d_1}^4 y^2} + \frac{b|\sin y| + c}{m_H l_0}\sin\alpha_0 \\
&= (1 - d_1\cos\alpha_0)\, y + \frac{b|\sin y| + c}{m_H l_0}\sin\alpha_0 \\
&= \sigma_1(y).
\end{aligned}$$

So $\sigma_2(0) > \sigma_1(0) > 0$.

For $y = -\frac{\pi}{2}$,

$$\begin{aligned}\sigma_2(-\frac{\pi}{2}) &= -\frac{\pi}{2} + \frac{\cos\alpha_0}{d_1}\sqrt{\frac{\pi^2 {d_1}^4}{4} + 2e_4\gamma_0 + \frac{\gamma_0^2}{d_2^2}} + \frac{b+c}{m_H l_0}\sin\alpha_0 \\ &< -\frac{\pi}{2} + \frac{\cos\alpha_0}{d_1}\sqrt{\frac{\pi^2 {d_1}^4}{4} + \frac{2\gamma_0^2}{d_2^2}} + \frac{b+c}{m_H l_0}\sin\alpha_0 \\ &< 0\end{aligned}$$

under condition (31) and

$$b < -\left[-\tfrac{\pi}{2} + \tfrac{\cos\alpha_0}{d_1}\sqrt{\tfrac{\pi^2 {d_1}^4}{4} + \tfrac{2\gamma_0^2}{d_2^2}}\right]\tfrac{m_H l_0}{\sin\alpha_0} - c := b_3. \tag{32}$$

It follows from $y \in (-\frac{\pi}{2},\ 0)$ and (31) that

$$\sqrt{{d_1}^4 y^2 + 2e_4\gamma_0 + \tfrac{\gamma_0^2}{d_2^2}} > \sqrt{2e_4\gamma_0 + \tfrac{\gamma_0^2}{d_2^2}} > -\tfrac{\gamma_0}{d_2},$$

$$\frac{y}{\sqrt{{d_1}^4 y^2 + 2e_4\gamma_0 + \frac{\gamma_0^2}{d_2^2}}} > \frac{\pi d_2}{2\gamma_0},$$

and

$$\sigma'_2(y) = 1 + d_1^3\cos\alpha_0\frac{y}{\sqrt{{d_1}^4 y^2 + 2e_4\gamma_0 + \frac{\gamma_0^2}{d_2^2}}} - \frac{b\cos y}{m_H l_0}\sin\alpha_0 > 0,$$

under condition

$$b < (1 + \tfrac{\pi d_1^3 d_2}{2\gamma_0}\cos\alpha_0)\tfrac{m_H l_0}{\sin\alpha_0} := b_4. \tag{33}$$

$\sigma_2(y)$ is monotonically increasing for $y \in \left(-\frac{\pi}{2}, 0\right)$.

For $y \in (0,\ +\infty)$, $\sigma'_2(y) >\ 0$ under condition $0 < b < b_4$. In view of $\sigma_2(0) > 0$, $\sigma_2(y) > 0$ for $y \in (0,\ +\infty)$.

For $y \in \left(-\infty,\ -\frac{\pi}{2}\right)$, we have

$$d_1^4\left(1 - d_1^2\cos^2\alpha_0\right)y^2 + 2e_4\gamma_0 + \frac{\gamma_0^2}{d_2^2} > 0,$$

$$1 + d_1^3\cos\alpha_0\frac{y}{\sqrt{{d_1}^4 y^2 + 2e_4\gamma_0 + \frac{\gamma_0^2}{d_2^2}}} >\ 0,$$

and $y + \frac{\cos\alpha_0}{d_1}\sqrt{{d_1}^4 y^2 + 2e_4\gamma_0 + \frac{\gamma_0^2}{d_2^2}}$ is monotonically increasing, so we obtain

$$\sigma_2(y) < y + \frac{\cos\alpha_0}{d_1}\sqrt{d_1^4 y^2 + 2e_4\gamma_0 + \frac{\gamma_0^2}{d_2^2}} + \frac{b+c}{m_H l_0}\sin\alpha_0$$

$$< \sigma_2(-\frac{\pi}{2}) < 0,$$

under condition $0 < b < b_3$.

There is only one root of equation $\sigma_2(y) = 0$ for $-\infty < y < +\infty$, which means that there is an unique fixed point in map (22) and hence there is an unique periodic gait in system (13) for $e_2 = \frac{\theta_0}{2}$, $e_4 \in \left(\frac{\gamma_0}{2d_2^2},\ 0\right)$, and $0 < b < \min\{b_3, b_4\}$. The following result is obtained.

Proposition 3. *Set $e_2 = \frac{\theta_0}{2}$, $e_4 \in \left(\frac{2}{3d_2}\gamma_0,\ 0\right)$ in system (13). There is an unique periodic gait for $0 < b < \min\{b_3,\ b_4\}$, where b_3 and b_4 are shown in (32) and (33), respectively.*

3.5. Stability and bifurcation of periodic gaits

As mentioned in the above subsection, one fixed point x_{3d} of map (21) corresponds to one periodic gait of (13). Now we discuss stability of this periodic gait of (13).

In view of (21), the eigenvalue of the fixed point x_{3d} is

$$\lambda_d = h'(x_{3d}) = -\frac{s_d(x_{3d}^2-\theta_0^2+2\theta_0 e_2)}{\sqrt{\frac{4Z_1^2}{d_2^2}+\frac{\gamma_0^2}{d_2^2}+2\gamma_0 e_4}} d_1^3 \cos(-\alpha_0) + \frac{br\cos x_{3d}+c}{m_H l_0}\sin(-\alpha_0), \tag{34}$$

where $r = \begin{cases} 1, & x_{3d} \in (-2n\pi,\ -(2n-1)\pi), \\ -1, & x_{3d} \in (-(2n-1)\pi,\ -2(n-1)\pi), \end{cases}$ $n \in \mathbb{N}$. The periodic gait of (13) is stable for $|\lambda_d| < 1$.

Proposition 2 shows that system (13) has an unique periodic gait for some conditions. It follows from map (22) that the eigenvalue of the fixed x_{3d} is

$$\lambda_d = h'(x_{3d1}) = d_1\cos\alpha_0 + \frac{b\cos x_{3d}}{m_H l_0}\sin\alpha_0. \tag{35}$$

This periodic gait is stable for $|\lambda_d| < 1$, namely

$$-1 < d_1\cos\alpha_0 + \frac{b\cos x_{3d}}{m_H l_0}\sin\alpha_0 < 1,$$

$$\frac{-1-d_1\cos\alpha_0}{\sin\alpha_0\cos x_{3d}} m_H l_0 < b < \frac{1-d_1\cos\alpha_0}{\sin\alpha_0\cos x_{3d}} m_H l_0.$$

Note that $\cos x_{3d} \in (0, 1)$, it follows that

$$\frac{m_H l_0}{\sin\alpha_0}(-1-d_1\cos\alpha_0) < b < \frac{m_H l_0}{\sin\alpha_0}(1-d_1\cos\alpha_0). \tag{36}$$

So system (12) has a unique stable period-1 gait for $b_2 - \frac{2m_H l_0}{\sin\alpha_0} < b < \min\{b_1,\ b_2\}$.

Let $(x_{3d},\ b_5)$ be the solution to the following equations.

$$\begin{cases} x_{3d} = d_1\cos\alpha_0\ x_{3d} - \frac{b|\sin x_{3d}|+c}{m_H l_0}\sin\alpha_0, \\ d_1\cos\alpha_0 + \frac{b\cos x_{3d}}{m_H l_0}\sin\alpha_0 = -1. \end{cases} \tag{37}$$

It follows from (35) that $\lambda_d = -1$ for $b = b_5$. An eigenvalue with -1 is associated with a flip bifurcation. So $(x_{3d},\ b_5)$ is a candidate for flip bifurcation point in map (22).

Now use the following lemma [27] to discuss the stability and direction of bifurcation of period-1 gait.

Lemma 1. *Let $f_\mu : R \to R$ be a one-parameter family of maps such that f_μ has a fixed point s_d with eigenvalue -1. Assume that the following two conditions hold.*

$$\frac{\partial f}{\partial \mu}\frac{\partial^2 f}{\partial^2 s} + 2\frac{\partial^2 f}{\partial \mu \partial s} \neq 0, \tilde{a} = \frac{1}{2}f_{ss}^2 + \frac{1}{3}f_{sss} \neq 0.$$

Then, there is a smooth curve of fixed points of f_μ passing through (s_d, μ_d), the stability of which changes at (s_d, μ_d). There is also a smooth curve β passing through (s_d, μ_d) so that $\beta \setminus (s_d, \mu_d)$ is a union of hyperbolic period-2 orbits.

In map (22), if the following condition holds,

$$\frac{\partial h}{\partial b}\frac{\partial^2 h}{\partial^2 x} + 2\frac{\partial^2 h}{\partial b \partial x} \neq 0, \ \tilde{a} = \frac{1}{2}h_{xx}^2 + \frac{1}{3}h_{xxx} > 0, \tag{38}$$

at $(b_5, \ x_{3d2})$, a flip bifurcation occurs at $b = b_5$. System (13) has a stable period-2 gait for $b \in (b_5, \ b_5 + \epsilon)$, where $\epsilon > 0$. Consequently, we obtain the following result.

Proposition 4. *Set $e_2 = \frac{\theta_0}{2}$, $e_4 = -\frac{\gamma_0}{2d_2^2}$ in system (13). There is an unique stable periodic gait for $b_2 - \frac{2m_H l_0}{\sin\alpha_0} < b < \min\{b_1, \ b_2\}$, where b_1 and b_2 are shown in (27) and (28), respectively. A flip bifurcation occurs at $b = b_5$ under condition (38) and system (13) has a stable period-2 gait for $b \in (b_5, \ b_5 + \epsilon)$, where $\epsilon > 0$ and b_5 is the solution to (37).*

4. Simulation results

To discuss the complex dynamics of system (13), the values of some parameters are given in Table I.

Table 1. The values of some parameters in system (13).

l_0	L_0	m	m_H	g	H	S
1	1.0787	0.5	10	0.98	0.1	0.64

Now first investigate the existence and stability of period-1 gaits of linearized system (13) with $\theta_0 = 0.6945 \ rad, \ \gamma_0 = -0.6351 \ rad$, and $c = 3$.

Set $u_2^* = e_2 = 0.34725, u_4^* = e_4 = 0.256$, $\gamma_1 = 0.4$. It follows from (16), (19), (27) and (28) that $u_1^* = -0.26$, $u_3^* = -0.12$, $b_1 \approx 9.59$, and $b_2 \approx 8.02$, respectively. Set $b = 4.8$, where $b < \min\{b_1, \ b_2\}$. System (13) has a period-1 gait, which starts from the initial point $A_d = (0.6945, \ -0.6351, \ -0.79, \ -0.16)^T$, reaches $B_d^- = (0, \ 0.4, \ -0.79, \ 2.08)^T$ at $t = \tau_1 = 0.94$, jumps to $B_d^+ = (0, \ 0.4, \ -0.68, \ 2.14)^T$, reaches $A_d^- = (-0.6351, \ 0.6945, \ -0.71, \ -1.7)^T$ at $t = \tau_1 + \tau_2 = 1.918$, and jumps to A_d. The portrait in $x_1 - x_3$ space and time series of x_i $(i = 1, 2, 3, 4)$ are shown in Figure 6, which is in agreement with Proposition 2.

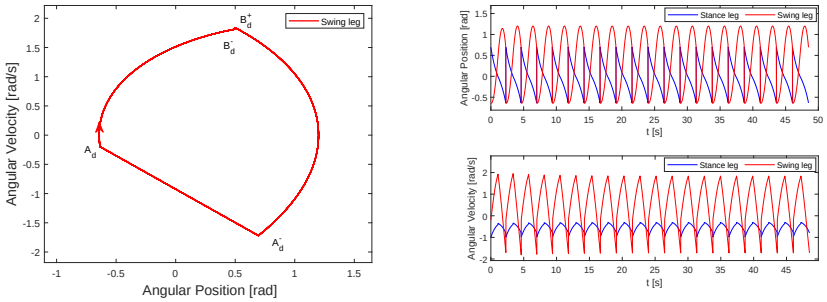

(a) (b)

Figure 6. For system (13) with $b = 4.8$, $c = 3$, $\gamma_1 = 0.4$, $u_1^* = -0.26$, $u_2^* = 0.34725$, $u_3^* = -0.12$, $u_4^* = 0.256$, (a) the period−1 gait in $x_2 - x_4$ space, (b) time series of x_i $(i = 1, 2, 3, 4)$.

Set $u_2^* = e_2 = 0.34725$, $u_4^* = e_4 = -0.07$, where $e_4 \in \left(\frac{2}{3d_2}\gamma_0,\ 0\right)$. It follows from (16), (19), (32) and (33) that $u_1^* = -0.275$, $u_3^* = 0.24$, $b_3 \approx 2.05$, $b_4 \approx 4.96$, respectively. Set $\gamma_1 = 0.9$, $b = 2$, where $0 < b < \min\{b_3,\ b_4\}$. As shown as Figure 7, system (13) has a period-1 gait, which is in agreement with Proposition 3.

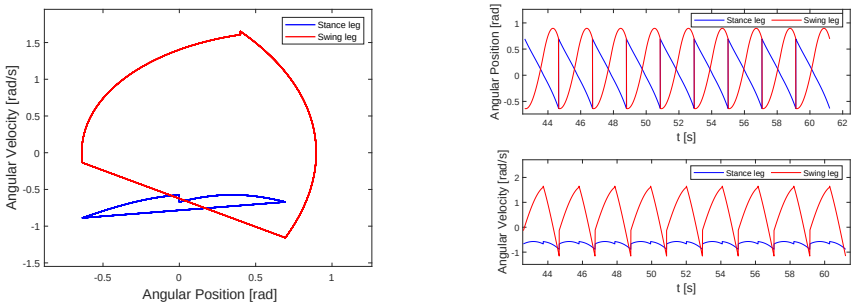

(a) (b)

Figure 7. For system (13) with $b = 2$, $c = 3$, $\gamma_1 = 0.9$, $u_1^* = -0.275$, $u_2^* = 0.34725$, $u_3^* = 0.24$, $u_4^* = -0.07$, (a) the period−1 gait in $x_1\ (x_3) - x_2\ (x_4)$ space, (b) time series of x_i $(i = 1, 2, 3, 4)$.

Set $b = 6.7$, $\gamma_1 = 0.4$, $u_1^* = 0.298$, $u_2^* = -0.25$, $u_3^* = 0.183$, $u_4^* = -0.13$. In view of the map (22), we can find $x_{3d_1} \approx -1.1$, $|\lambda_d| < 1$, and the fixed point $A_d = (0.6945,\ -0.6351,\ -1.1,\ -0.23)^T$ by numerical calculation. It's seen from Figure 8(a) that there exists a period-1 gait starting from A_d in system (13). In Figure 8(b), a gait starting from the point $(0.6945,\ -0.6351,\ -0.97,\ -0.195)^T$ tends to the period-1 gait with t increasing, which means that the period-1 gait is stable.

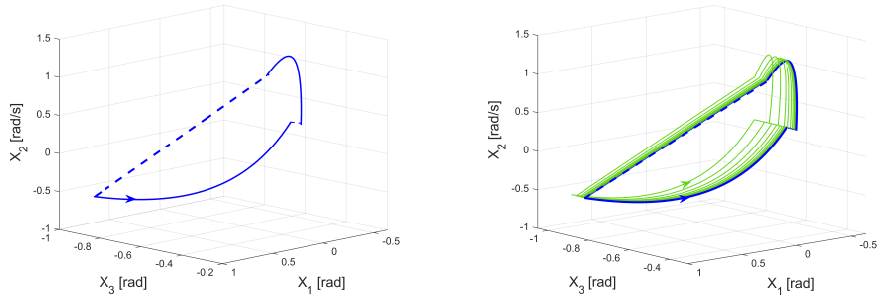

(a) (b)

Figure 8. For system (13) with $b = 6.7$, $c = 3$, $\gamma_1 = 0.4$, $u_1^* = 0.298$, $u_2^* = -0.25$, $u_3^* = 0.183$, $u_4^* = -0.13$, (a) the period-1 gait starting from A_d $(0.6945,\ -0.6351,\ -1.1,\ -0.23)^T$, (b) gaits starting from the points A_d and $(0.6945,\ -0.6351,\ -0.97,\ -0.195)^T$.

By viewing b as a parameter, the bifurcation diagram, which can well show the dynamic characteristics of system (13) with $(\theta_0, \gamma_0) = (0.6945,\ -0.6351)$, $c = 3$, $\gamma_1 = 0.4$, $u_2^* = -0.25$, $u_4^* = -0.13$, is shown in Figure 9. A period-2 gait bifurcates from the period-1 gait at $b \approx 19.095$ and the period-2 gait is stable for $b \in (19.095,\ 23.752)$. The numerical results shown in Figures 8 and 9 are in agreement with Proposition 4.

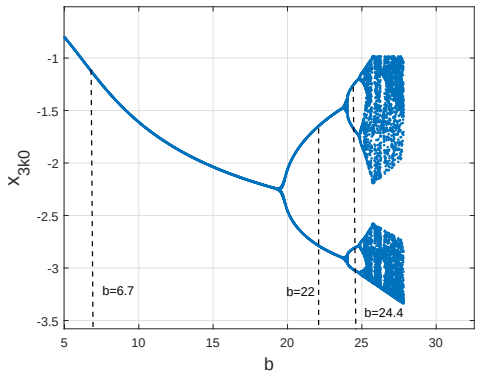

Figure 9. Bifurcation diagram of system (13) with $c = 3$, $\gamma_1 = 0.4$, $u_2^* = -0.25$, $u_4^* = -0.13$, $b \in [5,\ 28]$.

As shown in Figure 10(a)–(c), there exists a stable period-2 gait in system (13) with $b = 22$, $c = 3$, $\gamma_1 = 0.4$, $u_2^* = -0.25$, $u_4^* = -0.13$. In Figure 10(d), a gait starting from the point $(0.6945,\ -0.6351,\ -2.7,\ -0.547)^T$ tends to the period-1 gait with t increasing, which means that the period-2 gait is stable. The values of x_{3k0}, u_1^*, u_3^* of this period-2 gait of iteration number n are given in Figure 11.

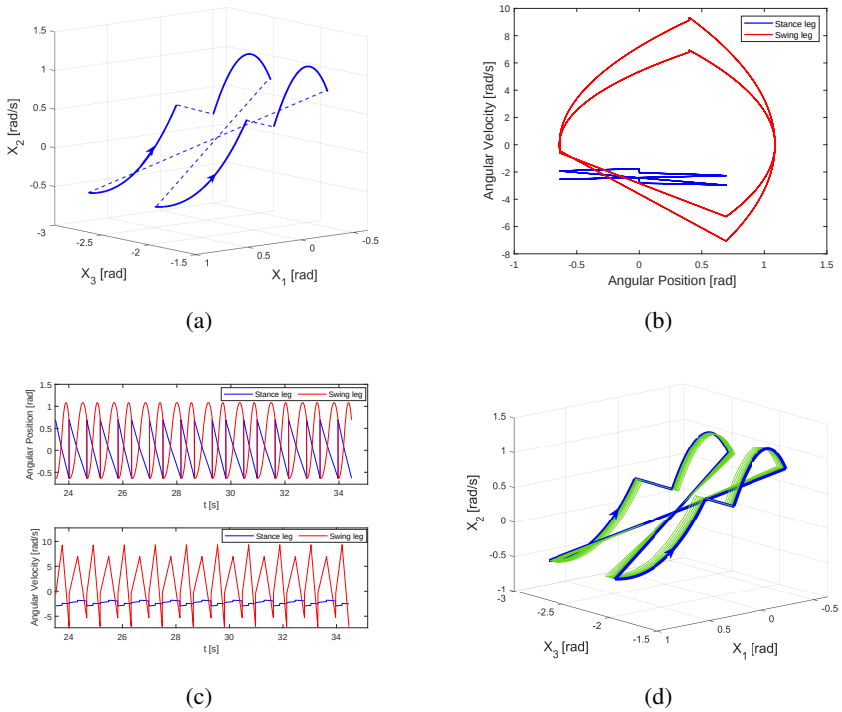

Figure 10. For system (13) with $b = 22$, $c = 3$, $\gamma_1 = 0.4$, $u_2^* = -0.25$, $u_4^* = -0.13$, (a) period-2 gait in the $x_1 - x_2 - x_3$ space, (b) period-2 gait in $x_1\,(x_3) - x_2\,(x_4)$ space, (c) time series of x_1 and x_3 and time series of x_2 and x_4, (d) period gait -2 and a gait starting from the point $(0.6945,\ -0.6351,\ -2.7,\ -0.547)^T$.

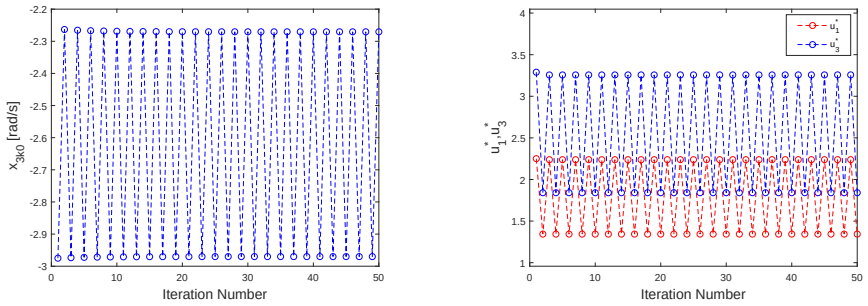

Figure 11. For linearized system (13) with $b = 22$, $c = 3$, $\gamma_1 = 0.4$, $u_2^* = -0.25$, $u_4^* = -0.13$, (a) values of x_{3k0} of iteration number n with $n = 50$, (b) values of u_1^*, u_3^* of iteration number n with $n = 50$.

Set $b = 24.4$, $c = 3$, $\gamma_1 = 0.4$, $u_2^* = -0.25$, $u_4^* = -0.13$. A period-4 gait is given in Figure 12.

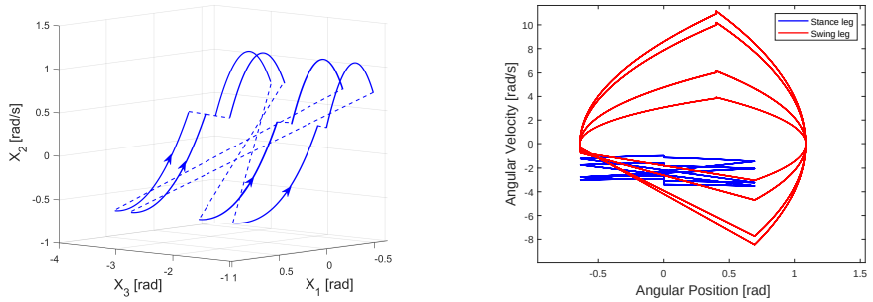

(a) (b)

Figure 12. For linearized system (13) with $b = 24.4$, $c = 3$, $\gamma_1 = 0.4$, $u_2^* = -0.3$, $u_4^* = -0.13$, (a) the period-4 gait in $x_1 - x_2 - x_3$ space, (b) period-4 gait in $x_1\,(x_3) - x_2\,(x_4)$ space.

Let $b = 26$ in system (13). Figure 13 shows a chaotic portrait of system (13) with $c = 3$, $\gamma_1 = 0.4$, $u_2^* = -0.25$, $u_4^* = -0.13$. The numerical results in Figures 10–13 are in agreement with bifurcation diagrams in Figure 9.

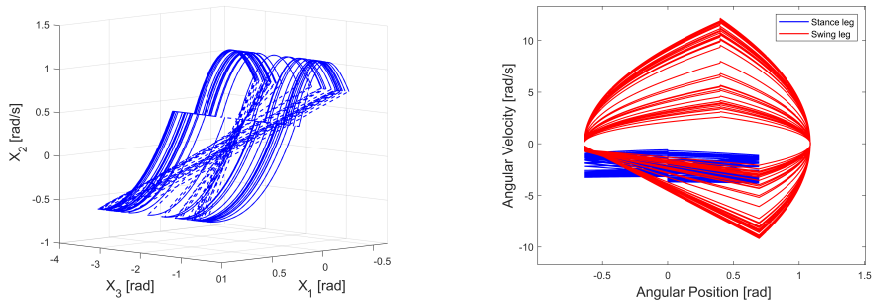

(a)

Figure 13. For linearized system (13) with $b = 26$, $c = 3$, $\gamma_1 = 0.4$, $u_2^* = -0.25$, $u_4^* = -0.13$,(a) the chaos gait in the $x_1 - x_2 - x_3$ space, (b) the chaos gait in $x_1\,(x_3) - x_2\,(x_4)$ space.

Now discuss the effect of torque on bifurcation of system (13). In Figure 9, a period-2 gait bifurcates from the period-1 gait at $b \approx 19.095$ for $u_2^* = -0.25$. Set $u_{2(1)}^* = 1.25$ and $u_{2(2)}^* = -1.25$. It's seen from Figure 14 that the occurrence of bifurcation is delayed to $b \approx 20.324$ for $u_{2(2)}^* = -1.25$ and advanced to $b \approx 18.653$ for $u_{2(1)}^* = 1.25$.

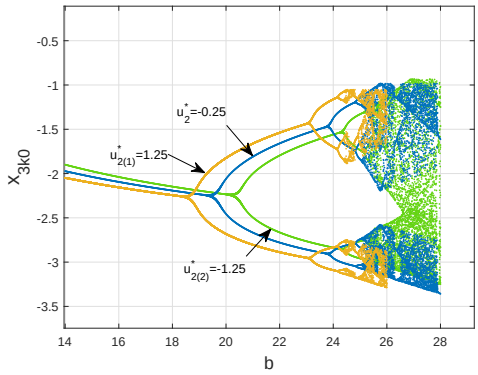

Figure 14. Bifurcation diagrams of system (13) with $c = 3$, $\gamma_1 = 0.4$, $u_2^* = -0.25$ ($u_{2(1)}^* = 1.25$, $u_{2(2)}^* = -1.25$), $u_4^* = -0.13$, $b \in [14,\ 28]$.

The above numerical results show that the linearized system (13) has complex dynamic behavior. Through the study of linearized system, we can roughly understand the dynamic properties of nonlinear system (9). For $b = 7.8$, $c = 3$, a stable period-1 gait of linearized system (9) is shown in Figure 7. When the parameters b and c are slightly disturbed, nonlinear system (9) still has a stable period-1 gait. Figure 15 shows a stable period-1 gait of nonlinear model for $b = 8.6$, $c = 3$, $u_1 = 3.32$, $u_2 = -2.5$, $u_3 = 2.4$ and $u_4 = -1.3$, where the fixed point is $X_d = [q^T,\ \dot{q}^T]^T = [0.6945,\ -0.6351,\ -1,\ -0.2037]^T$. Stick diagram of system (9) in Figure 16 clearly illustrates the process of ascending stairs of this robot.

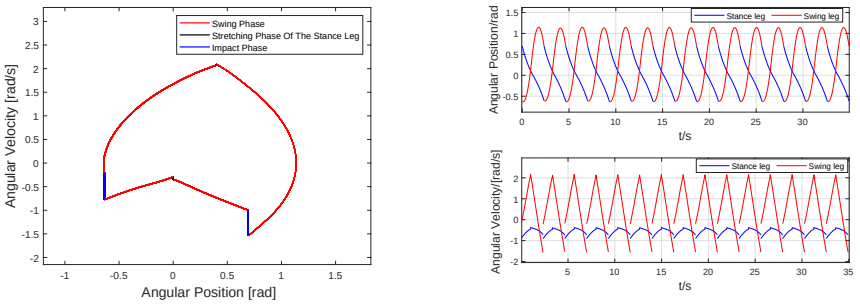

(a) (b)

Figure 15. For nonlinear system (9) with $b = 8.6$, $c = 3$, $u_1 = 3.32$, $u_2 = -2.5$, $u_3 = 2.4$ and $u_4 = -1.3$, (a) the period-1 gait in $x_1\,(x_3) - x_2\,(x_4)$ space, (b) time series of x_i $(i = 1, 2, 3, 4)$.

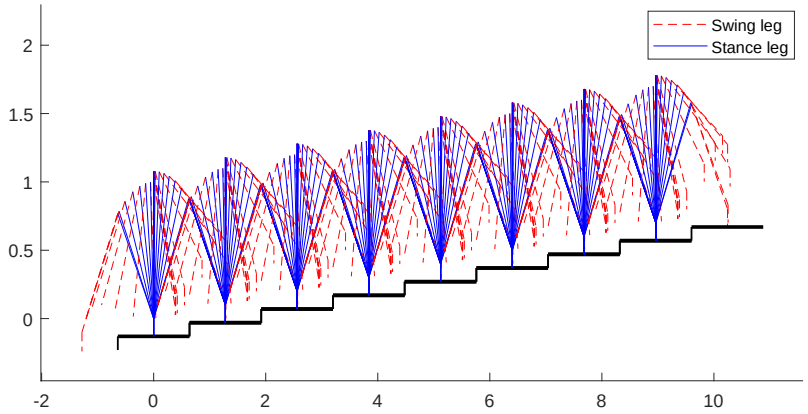

Figure 16. Stick diagram of system (9) with $b = 8.6$, $c = 3$, $u_1 = 3.32$, $u_2 = -2.5$, $u_3 = 2.4$ and $u_4 = -1.3$, and the initial point $[0.6945,\ -0.6351,\ -1,\ -0.2037]^T$.

The model of biped robot with knee joints [33] is more complex than that of straight legs biped robot. Now, we use the impulse thrust (20) to drive a biped robot with knee joints to walk upwards along slope. The walking process of this bipedal robot with knee joints is divided into four stages, namely, the knee-free phase, the knee strike phase, the knee-locked phase and heel strike. The modeling of up sloped bipedal robot with knee joints is shown in Appendix.

Set $a_1 = 0.375$, $a_2 = 0.175$, $b_1 = 0.125$, $b_2 = 0.325$, $m_s = 0.05$, $m_t = 0.5$, $m_h = 0.5$, $l_s = 0.5$, $l_t = 0.5, L = 1$, $u_1 = 3.2$, $u_2 = -0.27$, $u_3 = 0.003$ in this dynamic model of up sloped bipedal robot with knee joints. Set $b = 3.12$, $c = 1$ in impulse thrust (20). Figure 17 shows a stable period-1 gait of the up sloped bipedal robot with knee joints. The stick diagram Figure 18 clearly illustrates the process of walking upwards along a slope of this robot.

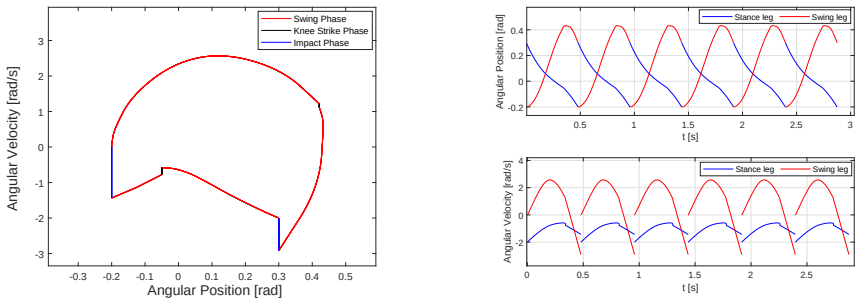

(a) (b)

Figure 17. For the up sloped bipedal robot with knee joints with $a_1 = 0.375$, $a_2 = 0.175$, $b_1 = 0.125$, $b_2 = 0.325$, $m_s = 0.05$, $m_t = 0.5$, $m_h = 0.5$, $l_s = 0.5$, $l_t = 0.5, L = 1$, $b = 3.12$, $c = 1$, (a) the period-1 gait, (b) time series of angular and angular angular velocity.

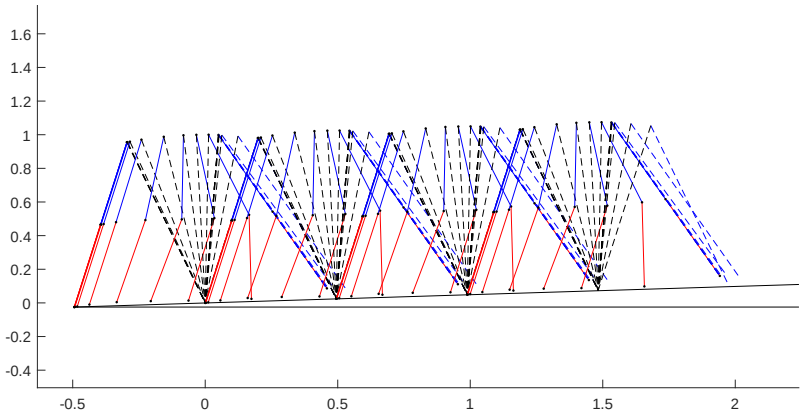

Figure 18. Stick diagram of the up sloped bipedal robot with knee joints with $a_1 = 0.375$, $a_2 = 0.175$, $b_1 = 0.125$, $b_2 = 0.325$, $m_s = 0.05$, $m_t = 0.5$, $m_h = 0.5$, $l_s = 0.5$, $l_t = 0.5$, $L = 1$, $b = 3.12$, $c = 1$, and the initial point $[0.3, -0.2, -0.2, -2, -0.0155, -0.0155]^T$. Black dotted lines for stance leg, red solid lines for swing shank, blue solids for the swing thigh and blue dotted lines for the swinging leg during the knee-lock phase.

5. Conclusions

In this study, telescopic legs and impulse thrust were considered to build a walking model of stair climbing biped robot. The nonlinear ascending stair biped model was linearized and an one-dimensional discrete map was obtained. The conditions for the existence and stability of period-1 gait were obtained by this one-dimensional discrete map. Flip bifurcation was investigated. Numerical simulation, such as phase diagram of period-1 gait, period-2 gait and period-4 gait, the bifurcation diagram, were given in an example.

The relationship among the torques u_i^* $(i = 1, 2, 3, 4)$ and the initial point $(\theta_0,\ \gamma_0,\ x_{3k0},\ x_{4k0})^T$ was investigated through theoretical analysis. We first give the initial point and the torques u_i^* $(i = 2, 4)$, and then calculate the value of u_i^* $(i = 1, 3)$, which enable two legs to exchange smoothly and ensure the realization of climbing stairs.

The parameter b play an important role in the ascending stair biped robot model. Proposition 4 gives the interval $\left(b_2 - \frac{2m_H l_0}{\sin\alpha_0},\ \min\{b_1,\ b_2\}\right)$ of parameter b that makes system has a stable period-1 gait in theory. Figure 9 shows that system has a stable period-1 gait for $b \in (5,\ 19.095)$. We can choose the appropriate value of b such that the stair climbing biped robot walk stably with period-1 gait.

We can adjust the value of torques to broaden the interval of parameter b of the existence of stable period-1 gait. Figure 14 shows that the interval of parameter b of the existence of stable period-1 gait is $b \in (5,\ 18.653)$, $b \in (5,\ 19.095)$, and $b \in (5,\ 20.324)$ for $u_2^* = 1.25$, $u_2^* = -0.25$, and $u_2^* = -1.25$, respectively. Obviously, under certain conditions, the larger the value of parameter u_2^*, the wider the interval of parameter b for the stair climbing biped robot to walk stably with period-1 gait.

Theoretical analysis and numerical simulation results obtained in this study provide a theoretical basis for stable walking of ascending stair biped robot with periodic gaits.

Acknowledgments

This work is jointly supported by the National Natural Science Foundation of China (11662001), the Science Foundation of Guangxi Province (2018GXNSFAA138177), the Young and Middle-aged Teachers Ability Promotion Project of Guangxi District (2019KY0228), and the Graduate innovation program of Guilin University of Electronic Technology (2021YCXS112).

Conflict of interest

The authors declare there is no conflicts of interest.

References

1. T. McGeer, Passive dynamic walking, *Int. J. Rob. Res.*, **9** (1990), 62–82. https://doi.org/10.1177/027836499000900206
2. S. Iqbal, X. Zang, Y. Zhu, J. Zhao, Bifurcations and chaos in passive dynamic walking, *Rob. Auton. Syst.*, **62** (2014), 889–909. https://doi.org/10.1016/j.robot.2014.01.006
3. B. Beigzadeh, S. Razavi, Dynamic walking analysis of an underactuated biped robot with asymmetric structure, *Int. J. Humanoid Rob.*, **18** (2021), 2150014. https://doi.org/10.1142/S0219843621500146
4. K. Deng, M. Zhao, W. Xu, Passive dynamic walking with a torso coupled via torsional springs, *Int. J. Humanoid Rob.*, **14** (2017), 1650024. https://doi.org/10.1142/S0219843616500249
5. K. Deng, M. Zhao, W. Xu, Level-ground walking for a bipedal robot with a torso via hip series elastic actuators and its gait bifurcation control, *Rob. Auton. Syst.*, **79** (2016), 58–71. https://doi.org/10.1016/j.robot.2016.01.013
6. D. Kerimoglu, O. Morgul, U. Saranli, Stability and control of planar compass gait walking with series-elastic ankle actuation, *Trans. Inst. Meas. Control*, **39** (2017), 312–323. https://doi.org/10.1177/0142331216663823
7. D. Maykranz, A. Seyfarth, Compliant ankle function results in landing-take off asymmetry in legged locomotion, *J. Theor. Biol.*, **349** (2014), 44–49. https://doi.org/10.1016/j.jtbi.2014.01.029
8. K. Zelik, T. Huang, P. Adamczyk, A. D. Kuo, The role of series ankle elasticity in bipedal walking, *J. Theor. Biol.*, **346** (2014), 75–85. https://doi.org/10.1016/j.jtbi.2013.12.014
9. T. Chen, J. Schmiedeler, B. Goodwine, Robustness and efficiency insights from a mechanical coupling metric for ankle-actuated biped robots, *Auton. Robot.*, **44** (2020), 281–295. https://doi.org/10.1007/s10514-019-09893-w
10. A. Kuo, Energetics of actively powered locomotion using the simplest walking model, *J. Biomech. Eng.*, **124** (2002), 113–120. https://doi.org/10.1115/1.1427703
11. Q. Ji, Z. Qian, L. Ren, L. Ren, Simulation analysis of impulsive ankle push-off on the walking speed of a planar biped robot, *Front. Bioeng. Biotechnol.*, **8** (2021), 621560. https://doi.org/10.3389/fbioe.2020.621560

12. D. Hobbelen, M. Wisse, Ankle actuation for limit cycle walkers, *Int. J. Rob. Res.*, **27** (2008), 709–735. https://doi.org/10.1177/0278364908091365

13. B. Wu, D. Qin, Y. Chen, T. Cao, M. Wu, Structure design of an omni-directional wheeled handling robot, *J. Phys. Conf. Ser.*, **1885** (2021), 052013.

14. P. Huang, Z. Zhang, X. Luo, J. Zhang, P. Huang, Path tracking control of a differential-drive tracked robot based on look-ahead distance, *IFAC-PapersOnLine*, **51** (2018), 112–117. https://doi.org/10.1016/j.ifacol.2018.08.072

15. Murshiduzzaman, T. Saleh, K. M. Raisuddin, Hexapod robot for autonomous machining, *IOP Conf. Ser.: Mater. Sci. Eng.*, **488** (2019), 012003. https://doi.org/10.1088/1757-899X/488/1/012003

16. T. Sato, S. Sakaino, E. Ohashi, K. Ohnishi, Walking trajectory planning on stairs using virtual slope for biped robots, *IEEE Trans. Ind. Electron.*, **58** (2011), 1385–1396. https://doi.org/10.1109/TIE.2010.2050753

17. C. Shih, Ascending and descending stairs for a biped robot, *IEEE Trans. Syst. Man Cybern. Part A Syst. Humans* , **29** (1999), 255–268. https://doi.org/10.1109/3468.759271

18. G. Figliolini, M. Ceccarelli, Climbing stairs with EP-WAR2 biped robot, in *IEEE International Conference on Robotics and Automation*, (2001), 4116–4121. https://doi.org/10.1109/ROBOT.2001.933261

19. G. Chen, J. Wang, L. Wang, Gait planning and compliance control of a biped robot on stairs with desired ZMP, *IFAC Proc. Vol.*, **47** (2014), 2165–2170. https://doi.org/10.3182/20140824-6-ZA-1003.02341

20. L. F. Cheng, K. Chen, Gait synthesis and sensory control of stair climbing for a humanoid robot, *IEEE Trans. Ind. Electron.*, **55** (2008), 2111–2120. https://doi.org/10.1109/TIE.2008.921205

21. M. Vatankhah, H. R. Kobravi, A. Ritter, Intermittent control model for ascending stair biped robot using a stable limit cycle model, *Rob. Auton. Syst.*, **121** (2019), 103255. https://doi.org/10.1016/j.robot.2019.103255

22. F. Asano, Z. W. Luo, S. Hyon, Parametric excitation mechanisms for dynamic bipedal walking, in *IEEE International Conference on Robotics & Automation*, (2006), 609–615. https://doi.org/10.1109/ROBOT.2005.1570185

23. S. Hasaneini, C. Macnab, J. Bertram, H. Leung, The dynamic optimization approach to locomotion dynamics: human-like gaits from a minimally-constrained biped model, *Adv. Rob.*, **27** (2013), 845–859. https://doi.org/10.1080/01691864.2013.791656

24. J. S. Moon, M. W. Spong, Bifurcations and chaos in passive walking of a compass-gait biped with asymmetries, in *IEEE International Conference on Robotics & Automation*, (2010), 1721–1726. https://doi.org/10.1109/ROBOT.2010.5509856

25. H. Gritli, S. Belghith, Walking dynamics of the passive compass-gait model under OGY-based control:emergence of bifurcations and chaos, *Commun. Nonlinear Sci. Numer. Simul.*, **47** (2017), 308–327. https://doi.org/10.1016/j.cnsns.2016.11.022

26. M. Fathizadeh, S. Taghvaei, H. Mohammadi, Analyzing bifurcation, stability and chaos for a passive walking biped model with a sole foot, *Int. J. Bifurcation Chaos*, **28** (2018), 1850113. https://doi.org/10.1142/S0218127418501134

27. X. Chen, Z. Jing, X. Fu, Chaos control in a pendulum system with excitations, *Discrete Contin. Dyn. Syst. Ser. B*, **20** (2015), 373–383. https://doi.org/10.3934/dcdsb.2015.20.373

28. W. Znegui, H. Gritli, S. Belghith, Design of an explicit expression of the Poincar map for the passive dynamic walking of the compass-gait biped model, *Chaos Solitons Fractals*, **130** (2020), 109436. https://doi.org/10.1016/j.chaos.2019.109436

29. F. Asano, Stability analysis of underactuated compass gait based on linearization of motion, *Multibody Syst. Dyn.*, **33** (2015), 93–111. https://doi.org/10.1007/s11044-014-9416-9

30. L. Li, Z. Xie, X. Luo, L. Li, Trajectory planning of flexible walking for biped robots using linear inverted pendulum model and linear pendulum model, *Sensors*, **21** (2021), 1082. https://doi.org/10.3390/s21041082

31. J. Ma, H. Jiang, Dynamics of a nonlinear differential advertising model with single parameter sales promotion strategy, *Electron. Res. Arch.*, **30** (2022), 1142–1157. https://doi.org/10.3934/era.2022061

32. X. Yang, J. Yu, H. Gao, An impulse control approach to spacecraft autonomous rendezvous based on genetic algorithms, *Neurocomputing*, **77** (2012), 189–196. https://doi.org/10.1016/j.neucom.2011.09.009

33. E. Added, H. Gritli, S. Belghith, Modeling and analysis of the dynamic walking of a biped robot with knees, in *2021 18th International Multi-Conference on Systems, Signals and Devices (SSD)*, (2021), 179–185. https://doi.org/10.1109/SSD52085.2021.9429493

Appendix

The description of a up sloped biped robot with knee joints

The model contains a hip joint and two legs with knee joints. The length of each leg is L which is divided into two parts ($L = l_s + l_t$), where l_s is the distance between the knee and the heel and l_t is the distance between the knee and the hip. For simplicity, we assume that the mass of the biped robot is distributed as three units, namely, shanks of two legs (m_s), shanks of two legs (m_t) and hip joint (m_h), where $m_h \gg m_s(m_h)$. Shanks and thighs are divided into two parts, $l_s = a_1 + b_1$ and $l_t = a_2 + b_2$, where a_1 (resp. b_1) is the distance between the sub-mass center ms and the heel (resp. knee), and a_2 (resp. b_2) is the distance between the sub-mass center m_t and the knee(resp. hip). The variables q_1, q_2 and q_3 represent the angles of the stance leg, the swing thigh and the swing shank relative to the ground of vertical, respectively.

Dynamic Model of the up sloped biped robot with knee joints

1) Knee-free phase

The following nonlinear dynamics of the biped robot during the knee-free swinging phases is

$$\mathcal{J}(q)\ddot{q} + \mathcal{H}(q,\dot{q})\dot{q} + \mathcal{G}(q) = B_3 u, \tag{39}$$

where $\mathcal{J}$ is the inertia matrix, $\mathcal{H}$ includes Coriolis and centrifugal terms, $\mathcal{G}$ includes gravity forces,

B_3 is the input matrix, u is the torque vector. They are given as follows.

$$\mathcal{J}(q) = \begin{bmatrix} \mathcal{J}_{11} & \mathcal{J}_{12} & \mathcal{J}_{13} \\ \mathcal{J}_{21} & \mathcal{J}_{22} & \mathcal{J}_{23} \\ \mathcal{J}_{31} & \mathcal{J}_{32} & \mathcal{J}_{33} \end{bmatrix},$$

$$\mathcal{H}(q,\dot{q}) = \begin{bmatrix} 0 & \mathcal{H}_{12}\dot{q}_2 & \mathcal{H}_{13}\dot{q}_3 \\ \mathcal{H}_{21}\dot{q}_1 & 0 & \mathcal{H}_{23}\dot{q}_3 \\ \mathcal{H}_{31}\dot{q}_1 & \mathcal{H}_{32}\dot{q}_2 & 0 \end{bmatrix},$$

$$\mathcal{G}(q) = \begin{bmatrix} \mathcal{G}_1 \\ \mathcal{G}_2 \\ \mathcal{G}_3 \end{bmatrix}, \quad B_3 = \begin{bmatrix} 1 & -1 & 0 \\ 0 & 1 & 0 \\ 0 & 0 & 1 \end{bmatrix}, \quad u = \begin{bmatrix} u_1 & u_2 & u_3 \end{bmatrix}^T,$$

$$\begin{aligned}
&\mathcal{J}_{11} = m_s a_1^2 + m_t(l_s + a_2)^2 + (m_h + m_s + m_t) L^2, \mathcal{J}_{12} = -(m_t b_2 + m_s l_t) L\cos(q_2 - q_1), \\
&\mathcal{J}_{13} = -m_s b_1 L\cos(q_3 - q_1), \mathcal{J}_{21} = \mathcal{J}_{12}, \\
&\mathcal{J}_{22} = m_t b_2^2 + m_s l_t^2, \mathcal{J}_{23} = m_s l_t b_1 \cos(q_3 - q_2), \\
&\mathcal{J}_{31} = \mathcal{J}_{13}, \mathcal{J}_{32} = \mathcal{J}_{23}, \mathcal{J}_{33} = m_s b_1^2, \\
&\mathcal{H}_{12} = -(m_t b_2 + m_s l_t) L\sin(q_1 - q_2), \mathcal{H}_{13} = -m_s b_1 L\sin(q_1 - q_3), \\
&\mathcal{H}_{21} = -\mathcal{H}_{12}, \mathcal{H}_{23} = m_s l_t b_1 \sin(q_3 - q_2), \\
&\mathcal{H}_{31} = -\mathcal{H}_{13}, \mathcal{H}_{32} = -\mathcal{H}_{23}, \\
&\mathcal{G}_1 = -(m_s a_1 + m_t(l_s + a_2) + (m_h + m_s + m_t) L) g\sin(q_1), \\
&\mathcal{G}_2 = (m_t b_2 + m_s l_t) g\sin(q_2), \mathcal{G}_3 = m_s b_1 g\sin(q_3),
\end{aligned}$$

where the torques u_1, u_2 and u_3 are applied to the hip joint, the ankle joints of stance during this phase and the knee of swing leg, respectively.

2) Knee strike phase

For the knee strike phase, the collision condition is

$$q_2 = q_3. \tag{40}$$

At the impact, a conservation of the angular momentum exists and leads to the following expression.

$$Q_1^+(q^+)\dot{q}^+ = Q_1^-(q^-)\dot{q}^-, \tag{41}$$

where $q^+ = \begin{bmatrix} q_1^+ & q_2^+ \end{bmatrix}^T$, $q^- = \begin{bmatrix} q_1^- & q_2^- & q_3^- \end{bmatrix}^T$, and

$$Q_1^+(q) = \begin{bmatrix} Q_{1,11}^+ Q_{1,12}^+ \\ Q_{1,21}^+ Q_{1,22}^+ \end{bmatrix}, Q_1^-(q) = \begin{bmatrix} Q_{1,11}^- Q_{1,12}^- Q_{1,13}^- \\ Q_{1,21}^- Q_{1,22}^- Q_{1,23}^- \end{bmatrix},$$

$$
\begin{aligned}
&Q^{+}_{1,11} = Q^{+}_{1,21} + m_t(l_s + a_2)^2 + (m_h + m_t + m_s)\, L^2 + m_s a_1^2, Q^{+}_{1,12} = Q^{+}_{1,21} + m_t(l_t + b_1)^2 + m_t b_2^2,\\
&Q^{+}_{1,22} = m_s(l_t + b_1)^2 + m_t b_2^2, Q^{-}_{1,11} = Q^{-}_{1,21} + (m_t + m_s + m_h)\, L^2 + m_s a_1^2 + m_t\,(l_s + a_2)^2,\\
&Q^{-}_{1,12} = -\,(m_s l_t + m_t b_2)\, L\cos(\alpha_1) + m_s b_1 l_t \cos(\alpha_3) + m_t b_2^2 + m_s l_t^2\\
&Q^{-}_{1,13} = -m_s b_1 L\cos(\alpha_2) + m_s b_1 l_t \cos(\alpha_3) + m_s b_1^2,\\
&Q^{-}_{1,21} = -\,(m_s l_t + m_t b_2)\, L\cos(\alpha_1) - m_s b_1 L\cos(\alpha_2)\,, Q^{-}_{1,22} = m_s b_1 l_t \cos(\alpha_3) + m_s l_t^2 + m_t b_2^2,\\
&Q^{-}_{1,23} = m_s b_1 l_t \cos(\alpha_3) + m_s b_1^2, \alpha_1 = q_1 - q_2\\
&\alpha_2 = q_1 - q_3,\\
&\alpha_3 = q_2 - q_3.
\end{aligned}
$$

3) Knee-locked phase
The moving pattern of this phase is similar to the third phase(III-IV) of the ascending stair biped robot, so the kinetic equation of this phase is similar to Eq (2).

4) Heel strike
For the heel strike phase, the collision condition is given by the following expression:

$$q_1 + q_2 - 2\varphi = 0, \tag{42}$$

where $\varphi(\varphi > 0)$ is the angle of the slope.
In this impact phase, impulse thrust p along the direction of the stance leg is used to provide the power. It follows that

$$\dot{q}_1^{+} = \dot{q}_1^{-}\cos(q_1^{-} - q_2^{-}) + \tfrac{p}{m_h L}\sin(q_1^{-} - q_2^{-}). \tag{43}$$

According to the momentum theorem, the following algebraic expression is obtained.

$$\dot{q}_2^{+} = (-m_s a_1\,(l_t + b_1) - m_t b_2\,(l_s + a_2))\,\dot{q}_2^{-} + (m_s\,(l_t + b_1) + m_t b_1)\,L\cos(q_1^{-} - q_2^{-})\dot{q}_1^{+}. \tag{44}$$